ACS OMEGA

http://pubs.acs.org/journal/acsodf

Article

Reduction in Work Functions of Transition-Metal Carbides and Oxycarbides upon Oxidation

Wataru Hayami,* Shuai Tang, Ta-Wei Chiu, and Jie Tang

Cite This: *ACS Omega* 2021, 6, 14559−14565

Read Online

ACCESS | Metrics & More | Article Recommendations

ABSTRACT: Herein, the work functions of group 4 and group 5 transition-metal (Ti, Zr, Hf, V, Nb, and Ta) carbides and transition-metal oxycarbides (TMCOs) were investigated by first-principles calculations for their potential application as electron emitters. The work functions of both groups decreased as the substitution of carbon atoms with oxygen proceeded, and the reduction in group 4 was more than that of group 5. In particular, $ZrC_{1-x}O_x$ and $HfC_{1-x}O_x$ ($x \geq 0.25$) exhibited work functions of less than 3 eV, which were comparable with those of LaB_6- and ZrO-coated tungsten. The reduction in the work functions could be explained by the rigid-band model of the electronic density of states. The increase in valence electrons increased the Fermi energy, while it demonstrated a less significant influence on the vacuum potential, resulting in a reduction in the work functions. The phonon dispersion curves indicated that the NaCl-type group 5 TMCOs were less stable than the group 4 TMCOs. This agrees with the experimental findings that $TaC_{1-x}O_x$ was not synthesized and $NbC_{1-x}O_x$ was synthesized only for smaller values of x (i.e., $x < 0.28$). From the viewpoints of the work functions and structural stabilities, group 4 (Ti, Zr, and Hf) TMCOs exhibit better potential for application as electron emitters than group 5 (V, Nb, and Ta) TMCOs.

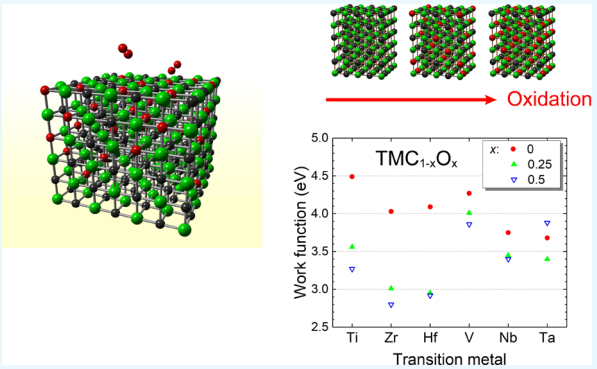

INTRODUCTION

Electron emission from solid surfaces has been a fundamental phenomenon known since the 19th century.[1,2] The electron gun was devised to generate an electron beam by accelerating the emitted electrons. It has been utilized in various instruments, such as cathode-ray tubes, electron microscopes, and electron beam lithography. The major types of electron guns are thermionic emission (TE), Schottky emission (SE), cold field emission (CFE), and thermal field emission (TFE). The electron source material has the most important role in electron guns, for which a variety of materials have been used. Currently, tungsten (W) (TE, CFE), LaB_6, and CeB_6 (TE), and tungsten coated with zirconium oxide (W/ZrO) (SE) are commercially used.[3−6]

The performance of electron guns is characterized by emission current (A), brightness ($A/m^2/sr$), stability, energy spread of the beam (eV), and the dimension of the emitter tip, which limits the image resolution. These factors are determined mainly by the work function of the electron-emitting material, the emitter tip profile, and the surface structure. Fundamentally, a lower work function and a sharper tip lead to better performance. The energy spread of the electron beam originates from the statistical distribution of the electron energy in the material. A material with a low work function enables the emitter to operate at low temperature, having a small energy spread.

The work functions of currently utilized W, LaB_6, and W/ZrO source materials are approximately 4.6,[7] 2.6,[8] and 2.7 eV,[5] respectively. From these values, LaB_6 and W/ZrO appear to be more advantageous than W. However, they are not suitable for CFE because their emission currents are not stable. An LaB_6 tip sharpened by electrochemical etching or other methods may be used for TFE.[9] For W/ZrO, the tip can be sharply pointed; however, when coated with ZrO, it undergoes dulling during operation.[10] For this reason, W is mainly used for the tip of a CFE-type emitter, whose dimensions must be less than 100 nm to generate a sufficiently intense electric field.

Despite the difficulty in precision fabrication, LaB_6 was successfully synthesized in the nanowire form by chemical vapor deposition (CVD),[11] the thickness of which was less than 100 nm. When applied to an electron emitter, the LaB_6 nanowire produced a stable CFE.[12,13]

LaB_6 is an excellent material that can produce a high-current and high-brightness electron beam. On the other hand, other

Received: March 29, 2021
Accepted: May 20, 2021
Published: May 27, 2021

materials that may show better performance and have lower production costs have been investigated for years. Metal carbides and nitrides are good candidates because they, like metal borides such as LaB_6, have metallic, covalent, and ionic bonds simultaneously.[14] There have been attempts to apply group 4 and 5 transition-metal carbides (TMCs) to an electron emitter.[15−22] Similar attempts have been made for transition-metal nitrides (TMNs).[23−30]

The probable reason why the LaB_6 nanowire was obtained using the CVD method is that LaB_6 has a cubic crystal structure whose surface energies greatly differ depending on the surface indices. The difference in the surface energy caused LaB_6 to grow along a specific direction ⟨100⟩.[12,13] In an analogous manner to LaB_6, we expected that group 4 and 5 TMCs could be made into nanowires because they also have a cubic structure (NaCl-type). Thus, we succeeded in fabricating HfC and ZrC nanowires growing in the ⟨100⟩ direction.[31−36]

When HfC and ZrC nanowires were applied to the electron emitters, they produced a stable CFE current. Notably, we found that the work function of the emitting surface {100}, which was originally approximately 3.6 eV for HfC[18] and ZrC,[17] greatly decreased when the wires were exposed to an oxygen atmosphere.[32,33] The work functions became approximately 2.5 eV for HfC[32] and 3.06 for ZrC,[33] which are close to the values for LaB_6 and W/ZrO. We also found that the emission currents of oxidized HfC and ZrC were stable for a long operation time (∼5 h). HfC and ZrC, therefore, have good potential as electron emitters.

Our previous studies showed that the surfaces of HfC and ZrC were partially oxidized, forming transition-metal oxycarbides (TMCOs) as they maintained the NaCl structure.[32,33] HfC and ZrC were spontaneously oxidized when exposed to an oxygen atmosphere at a high temperature. This implies that the compositions of oxycarbides can be controlled by the partial pressure of oxygen and the temperature of the sample. It is known that oxygen atoms can replace carbon atoms by up to approximately 50% in group 4 and 5 TMCs.[37−47] First-principles calculations showed that Hf and Zr oxycarbides could have lower work functions than those of the original carbides.[32,33] The stability of the emission current was probably caused by the passivation of the step edge, which prohibited further dissociative adsorption of residual gas molecules.

Thus far, we have investigated HfC and ZrC both experimentally and theoretically.[32,33] It is natural to extend the study to other group 4 (TiC) and 5 (VC, NbC, and TaC) TMCs to determine whether they show similar or better performance for electron emitters. In this study, we investigated these using first-principles calculations and found that there is a large difference in the work function and the structural stability between group 4 and group 5 TMCs. The difference and the mechanism of the reduction in work functions are discussed in terms of their atomic and electronic structures, and phonon dispersion relations, which will be provided in detail in the following sections.

RESULTS AND DISCUSSION

The work functions of TMCs and TMCOs were calculated using slab models, as depicted in Figure 1. In these models, the work functions were calculated on the (001) surfaces (top layers), which are intended to represent the {100} surfaces. Each model consists of (2 × 2 × 6) unit cells (96 atoms) and a vacuum space of 15 Å along the z direction (upward in the figure). The "x" in the figure denotes the ratio of oxygen in the chemical formula $TMC_{1-x}O_x$. In the TMCO models (x = 0.25 and 0.5), each layer has 16 atoms (8 TM and 8 C or O atoms), where the O atoms, denoted by red spheres in the figure, are uniformly distributed such that every layer has the same number of O atoms. The lattice constants and atomic positions were optimized for both TMC and TMCO when the lattice symmetry was constrained to an orthorhombic symmetry.

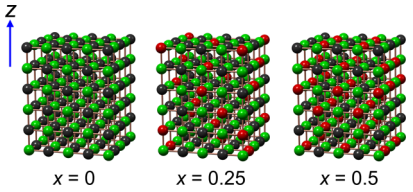

Figure 1. Slab models adopted in the calculations of the work functions of $TMC_{1-x}O_x$. Green, black, and red spheres depict TM, C, and O atoms, respectively. The work functions were calculated on the (001) surfaces (top layers), which represent the {100} surfaces.

Figure 2 shows the calculated work functions of the {100} surface of $TMC_{1-x}O_x$ (TM = Ti−Ta) at x = 0, 0.25, and 0.5.

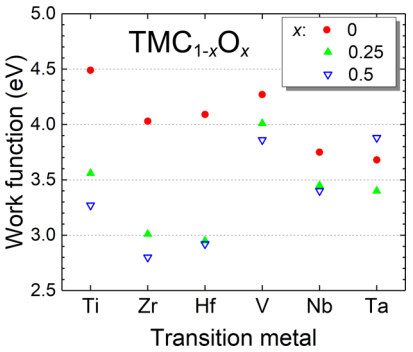

Figure 2. Calculated work functions of the {100} surfaces of $TMC_{1-x}O_x$.

The calculated values for TMCs (x = 0) are within approximately ±0.5 eV from experimental values,[48] and ±0.2 eV from theoretical values.[49−54] The differences from the experimental values are likely to be attributed to carbon defects in TMCs.[52−54] In the early stage of oxidation as x increases from 0 to 0.25, the work function greatly reduces for all these TMCs, which agrees well with our experimental results that the work function of HfC and ZrC reduces from 3.6 to 2.5 eV and from 3.6 to 3.02 eV, respectively.[32,33] In the case of $HfC_{1-x}O_x$, x was estimated to be approximately 0.2.[32] In the experiments,[31−36] the ⟨100⟩ oriented nanowires were sharpened by field evaporation when surfaces other than the {100} surface may have appeared. Even if other surfaces are involved in electron emission, the tendency would be the same because the reduction in work function is brought about mostly by the increase of the Fermi energy, as shown later in Figure 3.

As oxidation proceeds from 0.25 to 0.5, the work functions continue to decrease, but not as much as in the lower x range. Exceptionally, in the case of Ta, the work function increases slightly. This is probably related to its structural instability. In fact, the synthesis of NaCl-type TaCO has yet to be reported. The instability of TaCO is compared with that of HfCO later in terms of phonon dispersion curves (Figure 6).

Before oxidation, the group 4 TMCs tended to have a higher work function than the group 5 TMCs in the same row of the

https://doi.org/10.1021/acsomega.1c01671
ACS Omega 2021, 6, 14559−14565

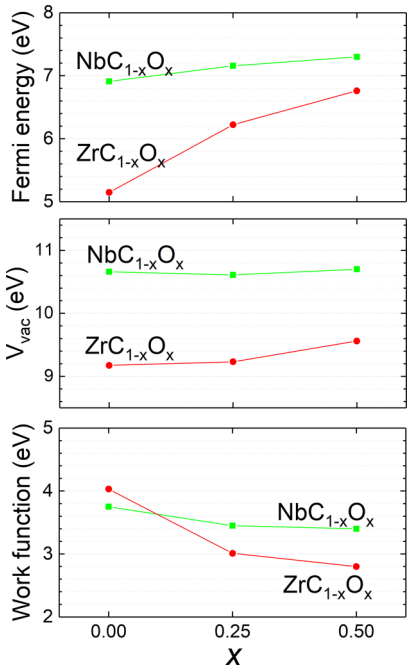

Figure 3. Fermi energies, vacuum potentials (V_{vac}), and work functions of $ZrC_{1-x}O_x$ and $NbC_{1-x}O_x$.

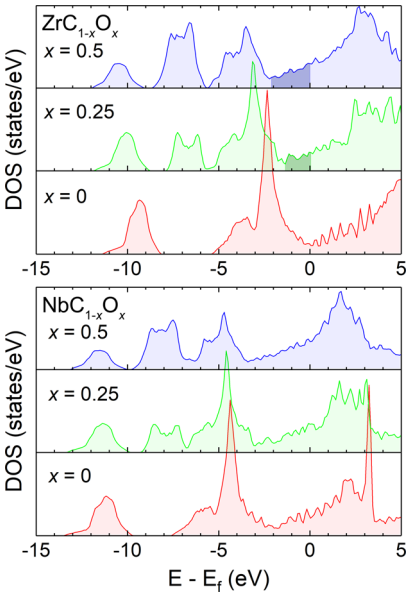

Figure 4. DOSs of $ZrC_{1-x}O_x$ (top) and $NbC_{1-x}O_x$ (bottom). The Fermi energies are set to zero.

periodic table, which is consistent with the results of previous studies.[49−51] However, the work functions of group 4 TMCOs were reduced by oxidation more effectively and became lower than those of group 5. On this point, group 4 TMCOs appear to be more advantageous than group 5 TMCOs.

To elucidate the difference in work function between group 4 and 5 TMCOs, the Fermi energies (E_fs), vacuum potentials (V_{vac}), and the work functions of ZrCO and NbCO were compared, as shown in Figure 3. The absolute value of the vacuum potential is not significant because it is dependent on the structural model adopted in the calculations. However, in the process of the oxidation of the TMCs, the same structural model was employed, except for the oxygen concentration. Thus, the relative change in the vacuum potential can be expected to reflect the change in the electric field due to the substitution of carbon by oxygen.

It was observed that for both ZrCO and NbCO, as x increased from 0 to 0.25, the E_f values increased, while the vacuum potentials were nearly the same. Because the work function is calculated from eq 1 in the Computational Methods section, the reduction in work function is caused for the most part by the increase in E_f in this x range. On the other hand, in the x range from 0.25 to 0.5, the increase in E_f is not as large as in the lower x range. At the same time, the vacuum potentials slightly increase, which cancels the increase in E_f in eq 1. Consequently, the work functions do not reduce significantly in the x range from 0.25 to 0.5.

The reason why the increase in E_f differs depending on x and the metal atoms can be explained by the densities of states (DOSs). We chose ZrCO and NbCO to represent group 4 and 5 TMCOs, and plotted their DOSs in Figure 4. The E_f values were set to zero. In the case of ZrCO (Figure 4, top), ZrC (x = 0) is semimetallic, and E_f is located at the bottom of the pseudogap. The DOSs at x = 0.25 and 0.5 appear to be similar to that at x = 0, except for the O 2p states in the region of −8 to −6 eV. The substitution of C with O atoms increases the number of valence electrons and accordingly increases E_f. The integrated DOSs from the bottom of the pseudogap to E_f (shadowed area) are 2.2 at x = 0.25 and 4.2 at x = 0.5, which nearly correspond to the increase of the valence electrons by the substitution. Therefore, the rigid-band model is valid for this substitution range.

When x = 0, because the DOS at E_f is low, the increase in valence electrons rapidly increases E_f. As E_f increases, the DOS at E_f gradually increases; therefore, the increase rate of E_f declines for the same increase in valence electrons. This explains the tendency of E_f in ZrCO shown in Figure 3.

The DOSs of NbCO (Figure 4, bottom) appear to be similar to those of ZrCO, and the rigid-band model still holds. The difference is that NbCO has one more valence electron, and accordingly has a higher E_f than ZrCO. Because the DOS at E_f is approximately 2.5 times higher than that in ZrCO, the increase rate of E_f for the increase in valence electrons should be 2.5 times lower than that in ZrCO, which explains the work function changes shown in Figure 2.

In Figure 3, it is observed that the vacuum potentials are nearly the same at x from 0 to 0.25, but slightly increase at x from 0.25 to 0.5. This behavior can be qualitatively explained by the electric field caused by the surface dipole moment. As shown in Figure 1, the {100} surface of the TMCs has the same number of TM and C atoms. The geometrically optimized {100} surface has C atoms located slightly outside the TM atoms. The relative z coordinates (RZC) of C and O to that of TM (Zr and Nb) are plotted in Figure 5, where the z direction is taken to be the outward direction normal to the surface. Because C and TM atoms have negative and positive charges, respectively, they generate inward electric dipole moments.

At x = 0.25, the RZC of C-TM is larger than that at x = 0, while that of O-TM is smaller than that of C-TM at x = 0 (Figure 5a). Therefore, the increase in the dipole moment is suppressed to a certain extent because the charges of the O and C atoms are comparable. In contrast, at x = 0.5, both the RZCs of C-TM and O-TM become larger than those of C-TM at x = 0, which greatly enhances the dipole moments. Taking the RZCs, electric charges, and atomic densities into account, the

https://doi.org/10.1021/acsomega.1c01671
ACS Omega 2021, 6, 14559−14565

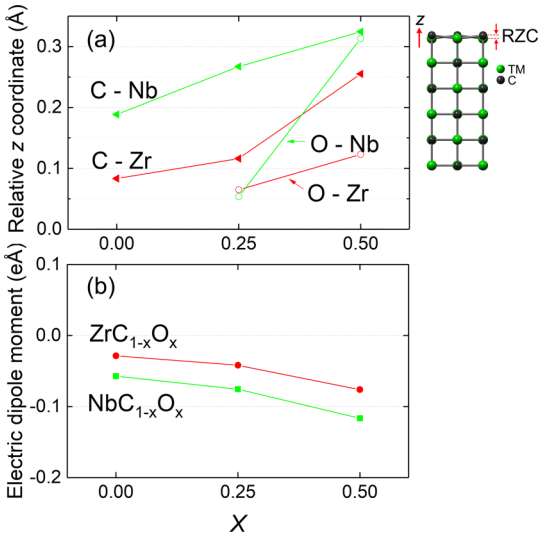

Figure 5. RZC of surface atoms (a), and the surface dipole moments (b) for $ZrC_{1-x}O_x$ and $NbC_{1-x}O_x$.

total electric dipole moments generated by the surface atoms are plotted in Figure 5b. The negative (inward) dipole moments generate an electric field that increases the vacuum potential, as shown in Figure 3.

At x from 0 to 0.25, the vacuum potentials are nearly unchanged (Figure 3), although the dipole moments slightly decrease. This difference probably originates from the electric field in the subsurface and the bulk, which we do not discuss in detail.

The RZCs for NbCO are larger than those for ZrCO (Figure 5a), which implies that NbCO (group 5) is less stable than ZrCO (group 4). This is understandable from their DOSs (Figure 4). E_f of NbC is located above the pseudogap, where the states have an antibonding character. $TMC_{1-x}O_x$, therefore, becomes less stable as x increases. In fact, the maximum x values for group 5 $TMC_{1-x}O_x$ (V, Nb, and Ta) obtained in experiments are 0.49 (V),[44] 0.28 (Nb),[45] and 0 (Ta). TaCO was observed only at the interface of TaC and TaO, but not in the bulk phase.[47] The instability of group 5 TMCOs is confirmed in terms of the phonon dispersion curves.

Figure 6 shows the phonon dispersion curves of $HfC_{1-x}O_x$ and $TaC_{1-x}O_x$. Before oxidation (x = 0), both HfC and TaC are stable, showing no imaginary phonon modes. As oxidation proceeds, $HfC_{1-x}O_x$ exhibits no imaginary modes until x = 0.5, whereas $TaC_{1-x}O_x$ has imaginary modes (presented by negative values) even at x = 0.25. The NaCl-type $TaC_{1-x}O_x$ is, therefore, unstable at x > 0.25, which agrees with the fact that the synthesis of bulk $TaC_{1-x}O_x$ has not been reported.[47]

Regarding VCO and NbCO, although their phonon dispersion curves have imaginary modes at x = 0.25 and 0.5 as observed in TaCO, oxygen substitution seems to be allowed to some extent. The maximum x for $NbC_{1-x}O_x$ is 0.28,[45] and that for $VC_{1-x}O_x$ is 0.49.[44] The value for $VC_{1-x}O_x$ is much larger than 0.25, and appears to be contradictory to the results of the phonon dispersion curves. This can probably be attributed to the nature of VC, in which the original VC has approximately 20% carbon defects.[44] The carbon defects, not included in the calculations, would help to stabilize the NaCl structure because the reduction in valence electrons lowers E_f toward the bottom of the pseudogap.

CONCLUSIONS

The work functions of group 4 (Ti, Zr, and Hf) and 5 (V, Nb, and Ta) TMCOs were investigated by first-principles calculations. For both groups, the work functions were reduced by the substitution of C atoms with O atoms, and those of

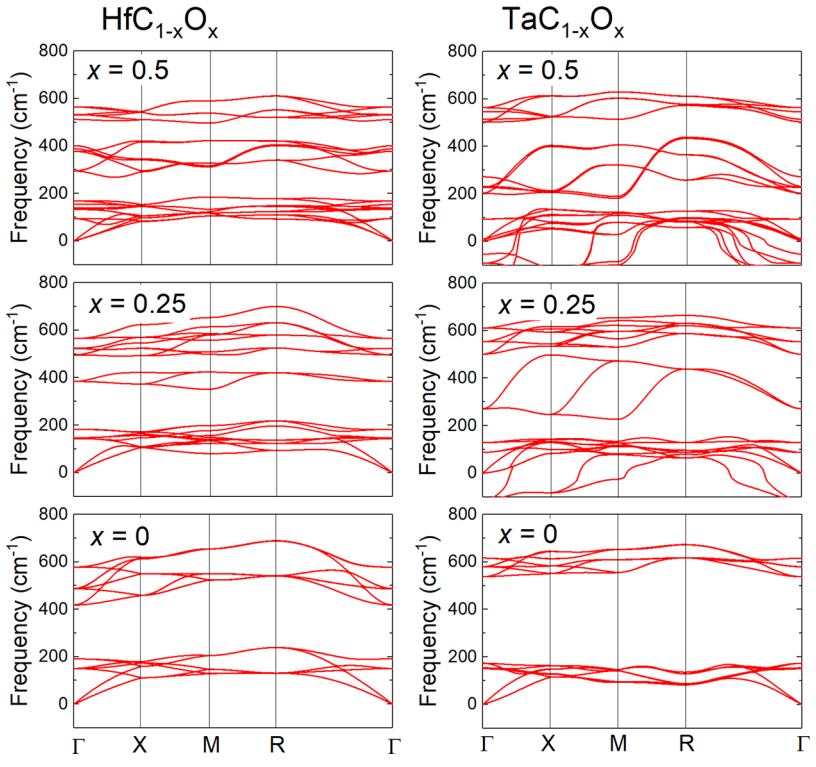

Figure 6. Calculated phonon dispersion curves of $HfC_{1-x}O_x$ and $TaC_{1-x}O_x$. Imaginary modes are represented by negative frequency values.

https://doi.org/10.1021/acsomega.1c01671
ACS Omega 2021, 6, 14559−14565

group 4 reduced more than those of group 5. In particular, $ZrC_{1-x}O_x$ and $HfC_{1-x}O_x$ ($x \geq 0.25$) exhibited a work function of less than 3 eV, suggesting that these materials have good potential as electron emitters.

The reduction in the work function is explained by the rigid-band model of the DOSs. As C atoms are replaced by O atoms, the number of valence electrons increases while the DOS spectrum maintains almost the same shape, which accordingly increases the values of E_f. In contrast, the vacuum potential was less influenced than E_f. As a result, the work function was reduced.

The phonon dispersion curves show that the NaCl-type group 5 TMCOs are less stable than the group 5 TMCOs. This agrees with the experimental findings that $TaC_{1-x}O_x$ has not been reported and $NbC_{1-x}O_x$ is reported only for small $x < 0.28$. Taking the work functions and stability into consideration, group 4 TMCOs have better potential for electron emitters than group 5 TMCOs.

COMPUTATIONAL METHODS

The electronic structures of TMCs and TMCOs were calculated using the Quantum ESPRESSO code,[55,56] based on density functional theory with plane waves and pseudopotentials. Scalar-relativistic ultrasoft pseudopotentials[57] for metals, carbon, and oxygen were adopted from the library.[58] The generalized-gradient-approximation functional of Perdew, Burke, and Ernzerhof was employed.[59] An energy cutoff of 60 Ry for plane waves and 600 Ry for electron density was sufficient to provide convergence of the total energy. The DOSs, work functions, and phonon dispersion curves were calculated following the optimization of the lattice parameters and the atomic structures using the Monkhorst−Pack k-point sampling[60] with an $(8 \times 8 \times 8)$ mesh per cubic unit cell. The calculated lattice parameters for the TMCs were within an error of 1% from the corresponding experimental values.

The work function ϕ was estimated using the following formula[61]

$$\phi = V_{vac} - E_f \quad (1)$$

where V_{vac} and E_f are the electrostatic potential of the vacuum and the Fermi energy, respectively.

The phonon dispersion curves were calculated based on the density functional perturbation theory[62] using the PHonon package in the Quantum ESPRESSO suite.

AUTHOR INFORMATION

Corresponding Author

Wataru Hayami − *International Center for Materials Nanoarchitectonics, National Institute for Materials Science, Tsukuba, Ibaraki 305-0044, Japan;* orcid.org/0000-0003-0497-8690; Email: HAYAMI.Wataru@nims.go.jp

Authors

Shuai Tang − *Center for Green Research on Energy and Environmental Materials, National Institute for Materials Science, Tsukuba, Ibaraki 305-0047, Japan*

Ta-Wei Chiu − *Center for Green Research on Energy and Environmental Materials, National Institute for Materials Science, Tsukuba, Ibaraki 305-0047, Japan*

Jie Tang − *Center for Green Research on Energy and Environmental Materials, National Institute for Materials Science, Tsukuba, Ibaraki 305-0047, Japan*

Complete contact information is available at: https://pubs.acs.org/10.1021/acsomega.1c01671

Notes

The authors declare no competing financial interest.

ACKNOWLEDGMENTS

The authors would like to thank Shigeki Otani for the valuable input and insightful comments. This work was supported partially by the NIMS-DENKA Center of Excellence for Next Generation Materials.

REFERENCES

(1) Becquerel, E. Rescherches Sur La Transmission De L'Electricite Au Travers Des Gaz A Des Temperatures Elevees. *Ann. Chim. Phys.* **1853**, *39*, 355−402.

(2) Guthrie, F. On a Relation Between Heat and Static Electricity. London, Edinburgh. *Dublin Philos. Mag. J. Sci.* **1873**, *46*, 257−266.

(3) Goebel, D. M.; Hirooka, Y.; Sketchley, T. A. Large-area lanthanum Hexaboride Electron Emitter. *Rev. Sci. Instrum.* **1985**, *56*, 1717−1722.

(4) Swanson, L. W.; Schwind, G. A. A Review of the Cold-Field Electron Cathode. *Adv. Imag. Electron. Phys.* **2009**, *159*, 63−100.

(5) Swanson, L.; Schwind, G. Review of ZrO/W Schottky Cathode. In *Handbook of Charged Particle Optics*, 2nd ed.; Orloff, J., Ed.; CRC Press: New York, 2008; Chapter 1, pp 1−28.

(6) Forbes, R. G. Gas Field Ionization Sources. In *Handbook of Charged Particle Optics*, 2nd ed.; Orloff, J., Ed.; CRC Press: New York, 2008; Chapter 3, pp 87−128.

(7) Michaelson, H. B. The Work Function of the Elements and its Periodicity. *J. Appl. Phys.* **1977**, *48*, 4729−4733 (W work function).

(8) Swanson, L. W.; McNeely, D. R. Work Functions of the (001) Face of the Hexaborides of Ba, La, Ce and Sm. *Surf. Sci.* **1979**, *83*, 11−28.

(9) Shimizu, R.; Kataoka, Y.; Tanaka, T.; Kawai, S. Field Emission Pattern of LaB_6-single Crystal Tip. *Jpn. J. Appl. Phys.* **1975**, *14*, 1089−1090.

(10) Bronsgeest, M. S. Physics of Schottky Electron Sources. Ph.D. Thesis, Technische Universiteit Delft, Netherlands, 2009. http://resolver.tudelft.nl/uuid:7975ef5e-c2ea-4056-be43-6bb6c062c884 (Schottky, dulling.

(11) Zhang, H.; Zhang, Q.; Tang, J.; Qin, L.-C. Single-Crystalline LaB_6 Nanowires. *J. Am. Chem. Soc.* **2005**, *127*, 2862−2863.

(12) Zhang, H.; Tang, J.; Zhang, Q.; Zhao, G.; Yang, G.; Zhang, J.; Zhou, O.; Qin, L.-C. Field Emission of Electrons from Single LaB_6 Nanowires. *Adv. Mater.* **2006**, *18*, 87−91.

(13) Zhang, H.; Tang, J.; Yuan, J.; Ma, J.; Shinya, N.; Nakajima, K.; Murakami, H.; Ohkubo, T.; Qin, L.-C. Nanostructured LaB_6 Field Emitter with Lowest Apical Work Function. *Nano Lett.* **2010**, *10*, 3539−3544.

(14) Lengauer, W. Transition Metal Carbides, Nitrides, and Carbonitrides. In *Handbook of Ceramic Hard Materials*; Riedel, R., Ed.; Wiley-VCH: Weinheim, Germany, 2000; p 202.

(15) Senzaki, K.; Kumashiro, Y. Field Emission Studies of TiC Single Crystal. *Jpn. J. Appl. Phys.* **1974**, *13*, 289−292.

(16) Adachi, H.; Fujii, K.; Zaima, S.; Shibata, Y.; Oshima, C.; Otani, S.; Ishizawa, Y. Stable Carbide Field Emitter. *Appl. Phys. Lett.* **1983**, *43*, 702−703.

(17) Mackie, W. A.; Hinrichs, C. H.; Davis, P. R. Preparation and Characterization of Zirconium Carbide Field Emitters. *IEEE Trans. Electron Devices* **1989**, *36*, 2691−2702.

(18) Mackie, W. A.; Lovell, J. M.; Curtis, T. W.; Magera, G. G. HfC(310) High Brightness Sources for Advanced Imaging Applications. *J. Vac. Sci. Technol. B* **2014**, *32*, 02B106.

(19) Back, T.; Fairchild, S. B.; Averett, K.; Maruyama, B.; Pierce, N.; Cahay, M.; Murray, P. T. Pulsed-Laser Deposited Transition-Metal Carbides for Field-Emission Cathode Coatings. *Appl. Mater. Interfaces* **2013**, *5*, 9241−9246.

(20) Liao, M. Y.; Gotoh, Y.; Tsuji, H.; Ishikawa, J. Deposition of Vanadium Carbide Thin Films using Compound Target Sputtering and their Field Emission. *J. Vac. Sci. Technol., A* **2005**, *23*, 1379−1383.
(21) Ishizawa, Y.; Aizawa, T.; Otani, S. Stable Field Emission and Surface Evaluation of Surface-processed NbC{110} Tips. *Appl. Surf. Sci.* **1993**, *67*, 36−42.
(22) Mackie, W. A.; Hartman, R. L.; Davis, P. R. High Current Density Field Emission From Transition Metal Carbides. *Appl. Surf. Sci.* **1993**, *67*, 29−35.
(23) Endo, M.; Nakane, H.; Adachi, H. Field Emission Characteristics of Transition-metal Nitrides. *J. Vac. Sci. Technol. B* **1996**, *14*, 2114−2118.
(24) Nagao, M.; Fujimori, Y.; Gotoh, Y.; Tsuji, H.; Ishikawa, J. Emission Characteristics of ZrN Thin Film Field Emitter Array Fabricated by Ion Beam Assisted Deposition Technique. *J. Vac. Sci. Technol. B* **1998**, *16*, 829−832.
(25) Lee, D.-G.; Baik, D.-K.; Kang, N.-S.; Cho, W.-K.; Yoon, S.-J.; Kim, T.-Y.; Hwang, H.-D.; Ahn, D.-H.; Park, M.-H. Fabrication of Volcano-type TiN Field Emitter Arrays. *J. Vac. Sci. Technol. B* **2000**, *18*, 1085−1088.
(26) Lo, W. K.; Parthasarathy, G.; Lo, C. W.; Tanenbaum, D. M.; Craighead, H. G.; Isaacson, M. S. Titanium Nitride Coated Tungsten Cold Field Emission Sources. *J. Vac. Sci. Technol. B* **1996**, *14*, 3787−3791.
(27) Ikeda, K.; Ohue, W.; Endo, K.; Gotoh, Y.; Tsuji, H. Development of a Vacuum Transistor using Hafnium Nitride Field Emitter Arrays. *J. Vac. Sci. Technol. B* **2011**, *29*, 02B116.
(28) Hu, Y.; Huo, K.; Ma, Y.; Lü, Y.; Xu, J.; Hu, Z.; Chen, Y. Synthesis and Field Emission Characterization of Titanium Nitride Nanowires. *J. Nanosci. Nanotechnol.* **2007**, *7*, 2922−2926.
(29) Chen, T.-M.; Hung, J.-Y.; Pan, F.-M.; Chang, L.; Sheu, J.-T.; Wu, S.-C. Fabrication and Field-Emission Characteristics of TiN Nanorods with a Concave Top Surface. *Electrochem. Solid-State Lett.* **2008**, *11*, K40−K43.
(30) Tao, Y.; Gao, Q.; Wang, X.; Wu, X.; Mao, C.; Zhu, J. NbN and NbS Nanobelt Arrays: In-Situ Conversion Preparation and Field-Emission Performance. *J. Nanosci. Nanotechnol.* **2011**, *11*, 3345−3349.
(31) Yuan, J.; Zhang, H.; Tang, J.; Shinya, N.; Nakajima, K.; Qin, L.-C. Field Emission from Single-crystalline HfC Nanowires. *Appl. Phys. Lett.* **2012**, *100*, 113111.
(32) Tang, S.; Tang, J.; Chiu, T.-W.; Hayami, W.; Uzuhashi, J.; Ohkubo, T.; Uesugi, F.; Takeguchi, M.; Mitome, M.; Qin, L.-C. A HfC Nanowire Point Electron Source with Oxycarbide Surface of Lower Work Function for High-brightness and Stable Field-emission. *Nano Res.* **2020**, *13*, 1620−1626.
(33) Chiu, T.-W.; Tang, J.; Tang, S.; Hayami, W.; Yuan, J.; Qin, L.-C. Reduced Work Function and Improved Field Emission Stability of ZrC Nanowires upon Surface Oxidation. *Appl. Phys. Lett.* **2020**, *117*, 053101.
(34) Tang, S.; Tang, J.; Chiu, T.-W.; Uzuhashi, J.; Tang, D.-M.; Ohkubo, T.; Mitome, M.; Uesugi, F.; Takeguchi, M.; Qin, L.-C. A Controllable and Efficient Method for Making Single HfC Nanowire Field-Emission Point Electron Source Aided by Low Kev FIB Milling. *Nanoscale* **2020**, *12*, 16770−16774.
(35) Chiu, T.-W.; Tang, J.; Tang, S.; Yuan, J.; Qin, L.-C. Growth and Field-Emission of Single-Crystalline Hafnium Carbide Nanowire. *Phys. Status Solidi A* **2020**, *217*, 2000007.
(36) Chiu, T.-W.; Tang, J.; Tang, S.; Yuan, J.; Qin, L.-C. Synthesis and Field Emission of ZrC Nanowire. *Mater. Today Commun.* **2020**, *25*, 101240.
(37) Oshima, C.; Otani, S.; Aono, M.; Zaima, S.; Shibata, Y. Titanium Oxycarbide on TiC(100) Surface. *Jpn. J. Appl. Phys.* **1983**, *22*, 930−933.
(38) Shimada, S. A Thermoanalytical Study of Oxidation of TiC by Simultaneous Tga-Dta-Ms Analysis. *J. Mater. Sci.* **1996**, *31*, 673−677.
(39) Jiang, B.; Huang, K.; Cao, Z.; Zhu, H. Thermodynamic Study of Titanium Oxycarbide. *Metall. Mater. Trans. A* **2012**, *43*, 3510−3514.
(40) Klimashi, G. M.; Kozlovsk, L. V.; Tszyu, A. K. Region of Oxycarbide-Phase Occurrence in Zr-C-O System. *Zh. Prikl. Khim.* **1971**, *44*, 1644.
(41) Shimada, S.; Inagaki, M.; Suzuki, M. Microstructural Observation of the ZrC/ZrO2 Interface Formed by Oxidation of ZrC. *J. Mater. Res.* **1996**, *11*, 2594−2597.
(42) Réjasse, F.; Rapaud, O.; Trolliard, G.; Masson, O.; Maître, A. Experimental Investigation and Thermodynamic Evaluation of the C-Hf-O Ternary System. *J. Am. Ceram. Soc.* **2017**, *100*, 3757−3770.
(43) Alyamovskii, S. I.; Zainulin, Y. G.; Shveikin, G. P.; Geld, P. V. Cubic Hafnium Oxycarbide. *Zh. Prikl. Khim.* **1971**, *16*, 1480.
(44) Zainulin, Y. G.; Dyachkova, T. V.; Alyamovskii, S. I. Electrical-Resistance of Vanadium Oxycarbides. *Inorg. Mater.* **1980**, *16*, 1476−1478.
(45) D'yachkova, T. V.; Alyamovskii, S. I.; Zainulin, Y. G. Effect of High-Pressures on the Structure and Properties of Niobium Oxycarbides. *Inorg. Mater.* **1987**, *23*, 56−60.
(46) daSilva, V.; Schmal, M.; Oyama, S. T. Niobium Carbide Synthesis from Niobium Oxide: Study of the Synthesis Conditions, Kinetics, and Solid-State Transformation Mechanism. *J. Solid State Chem.* **1996**, *123*, 168−182.
(47) Desmaison-Brut, M.; Alexandre, N.; Desmaison, J. Comparison of the Oxidation Behaviour of Two Dense Hot Isostatically Pressed Tantalum Carbide (TaC and Ta_2C) Materials. *J. Eur. Ceram. Soc.* **1997**, *17*, 1325−1334.
(48) Yoshitake, M. Generic Trend of Work Functions in Transition-metal Carbides and Nitrides. *J. Vac. Sci. Technol., A* **2014**, *32*, 061403.
(49) Viñes, F.; Sousa, C.; Liu, P.; Rodriguez, J. A.; Illas, F. A Systematic Density Functional Theory Study of the Electronic Structure of Bulk and (001) Surface of Transition-Metals Carbides. *J. Chem. Phys.* **2005**, *122*, 174709.
(50) Quesne, M. G.; Roldan, A.; de Leeuw, N. H.; Catlow, C. R. A. Bulk and Surface Properties of Metal Carbides: Implications for Catalysis. *Phys. Chem. Chem. Phys.* **2018**, *20*, 6905−6916.
(51) Hugosson, H. W.; Eriksson, O.; Jansson, U.; Ruban, A. V.; Souvatzis, P.; Abrikosov, I. A. Surface Energies and Work Functions of the Transition Metal Carbides. *Surf. Sci.* **2004**, *557*, 243−254.
(52) Rimsza, J. M.; Foiles, S.; Michael, J.; Mackie, W.; Larson, K. Role of Defects on the Surface Properties of HfC. *Appl. Surf. Sci.* **2019**, *495*, 143500.
(53) Price, D. L.; Cooper, B. R.; Wills, J. M. Effect of Carbon Vacancies on Carbide Work Functions. *Phys. Rev. B: Condens. Matter Mater. Phys.* **1993**, *48*, 15311−15315.
(54) Gruzalski, G. R.; Lui, S.-C.; Zehner, D. M. Work-Function Changes Accompanying Changes in Composition of (100) Surfaces of HfC, and TaC. *Surf. Sci. Lett.* **1990**, *239*, L517−L520.
(55) Giannozzi, P.; Baroni, S.; Bonini, N.; Calandra, M.; Car, R.; Cavazzoni, C.; Ceresoli, D.; Chiarotti, G. L.; Cococcioni, M.; Dabo, I.; Dal Corso, A.; de Gironcoli, S.; Fabris, S.; Fratesi, G.; Gebauer, R.; Gerstmann, U.; Gougoussis, C.; Kokalj, A.; Lazzeri, M.; Martin-Samos, L.; Marzari, N.; Mauri, F.; Mazzarello, R.; Paolini, S.; Pasquarello, A.; Paulatto, L.; Sbraccia, C.; Scandolo, S.; Sclauzero, G.; Seitsonen, A. P.; Smogunov, A.; Umari, P.; Wentzcovitch, R. M. Quantum Espresso: A Modular and Open-Source Software Project for Quantum Simulations of Materials. *J. Phys.: Condens. Matter* **2009**, *21*, 395502.
(56) Giannozzi, P.; Andreussi, O.; Brumme, T.; Bunau, O.; Buongiorno Nardelli, M.; Calandra, M.; Car, R.; Cavazzoni, C.; Ceresoli, D.; Cococcioni, M.; Colonna, N.; Carnimeo, I.; Dal Corso, A.; de Gironcoli, S.; Delugas, P.; DiStasio, R. A., Jr; Ferretti, A.; Floris, A.; Fratesi, G.; Fugallo, G.; Gebauer, R.; Gerstmann, U.; Giustino, F.; Gorni, T.; Jia, J.; Kawamura, M.; Ko, H.-Y.; Kokalj, A.; Küçükbenli, E.; Lazzeri, M.; Marsili, M.; Marzari, N.; Mauri, F.; Nguyen, N. L.; Nguyen, H.-V.; Otero-de-la-Roza, A.; Paulatto, L.; Poncé, S.; Rocca, D.; Sabatini, R.; Santra, B.; Schlipf, M.; Seitsonen, A. P.; Smogunov, A.; Timrov, I.; Thonhauser, T.; Umari, P.; Vast, N.; Wu, X.; Baroni, S. Advanced Capabilities for Materials Modelling with Quantum ESPRESSO. *J. Phys.: Condens. Matter* **2017**, *29*, 465901.

https://doi.org/10.1021/acsomega.1c01671
ACS Omega 2021, 6, 14559−14565

(57) Vanderbilt, D. Soft self-consistent Pseudopotentials in a Generalized Eigenvalue Formalism. *Phys. Rev. B: Condens. Matter Mater. Phys.* **1990**, *41*, 7892−7895.
(58) *Quantum ESPRESSO*. Home Page. http://www.quantum-espresso.org.
(59) Perdew, J. P.; Burke, K.; Ernzerhof, M. Generalized Gradient Approximation Made Simple. *Phys. Rev. Lett.* **1996**, *77*, 3865−3868.
(60) Monkhorst, H. J.; Pack, J. D. Special Points for Brillouin-zone Integrations. *Phys. Rev. B: Condens. Matter Mater. Phys.* **1976**, *13*, 5188−5192.
(61) Liu, W.; Zheng, W. T.; Jiang, Q. First-principles Study of the Surface Energy and Work function of III-V Semiconductor Compounds. *Phys. Rev. B: Condens. Matter Mater. Phys.* **2007**, *75*, 235322.
(62) Baroni, S.; de Gironcoli, S.; Dal Corso, A.; Giannozzi, P. Phonons and Related Properties of Extended Systems from Density Functional Perturbation Theory. *Rev. Mod. Phys.* **2001**, *73*, 515−562.

https://doi.org/10.1021/acsomega.1c01671
ACS Omega 2021, 6, 14559−14565